Water Research X 32 (2026) 100563

Contents lists available at ScienceDirect

Water Research X

journal homepage: www.sciencedirect.com/journal/water-research-x

Temporal evolution of hydrochemical changes in an acid mine drainage–impacted river using SWAT modeling and concentration–discharge relationships

Raúl Moreno-González [a,*], Manuel Olías [b], Carlos R. Cánovas [b], Laura Galván [c], Rubén Fernández de Villarán [c]

[a] Department of Earth Sciences and Institute for Marine Research (INMAR), University of Cadiz, Campus Rio San Pedro, s/n, 11510, Puerto Real, Spain
[b] Department of Earth Sciences & Research Center on Natural Resources, Health and the Environment. University of Huelva, Campus "El Carmen", E-21071, Huelva, Spain
[c] Department of Agroforestry Sciences, University of Huelva, Campus "El Carmen", E-21071 Huelva, Spain

ARTICLE INFO

Keywords:
Tinto river
Iberian pyrite belt
Sulfide mining
Trace elements
SWAT

ABSTRACT

The Tinto River is heavily polluted by historical sulfide mining, showing acidic conditions and extremely high concentrations of metals and metalloids along its 101 km course. The Riotinto mine closed in 2000 and was reopened in 2015, with a commitment to reduce acidic discharges from legacy mining wastes. This study assesses the effect of the 2015 reopening on pH and dissolved sulfate, metal and metalloid concentrations in the Tinto River, using a 2008–2021 dataset from a monitoring point 13 km downstream of the main mining area. Because no gauging station exists at this site, the Soil and Water Assessment Tool (SWAT) was applied to reconstruct continuous daily discharge and support concentration–discharge (C-Q) analyses. The pH remained consistently low (≈2.5), whereas dissolved species varied widely, with median concentrations of 3.45 g/L sulfate, 834 mg/L Fe and 59 mg/L Zn. The 2015–2021 period after the mine reopening was clearly drier than previous years. This should have produced an increased in dissolved concentrations through time. Nevertheless, the dissolved concentration of most elements showed slight downward trends, indicating reduced pollutant inputs from the mining areas, whereas Pb remained unchanged and Fe and As showed slight upward trends. For most elements concentration-discharge (CQ) relationships showed a dilution pattern with lower concentrations during 2015–2021, also suggesting improved water quality. Fe, As, and Pb showed the most complex behavior, as their concentrations are controlled by precipitation and coprecipitation processes. These results demonstrate that integrating hydrological modelling with long-term hydrochemistry datasets provides a robust framework to assess remediation effectiveness while accounting for the variability of climatic regimes.

1. Introduction

The Tinto River (SW Spain) represents one of the most extreme examples of acid mine drainage (AMD) pollution worldwide. A large part of its drainage basin lies within the Iberian Pyrite Belt (IPB), a region hosting extensive sulfide deposits that have been intensively exploited for copper and other raw materials (Olías et al., 2020). Historical mining activities have left abundant sulfide-rich wastes in the area, which undergo oxidation upon exposure to water and oxygen, generating acidity and releasing sulfate, iron, and other elements such as Pb, Zn, Cu, Cd, and As into the aquatic environment (Nordstrom et al., 2015).

Until the 1980s, environmental protection legislation in Spanish mining areas was largely absent, and mining companies were not required to implement measures to prevent the generation of acidic drainage. As a result, intensive mining activities, particularly since the mid-19th century in the Riotinto mining district, have left an area of 10.7 km^2 with sulfide-rich wastes in the headwaters of the Tinto River (Grande et al., 2013). Combined with the low neutralization capacity of the host rocks of the IPB, this legacy results in persistently acidic conditions and extremely high concentrations of sulfate, metals, and metalloids along nearly 100 km of the river, from its headwaters to its mouth in the Huelva Estuary (Fig. 1). This contamination also severely affects

* Corresponding author.
E-mail address: raul.morenogonzalez@uca.es (R. Moreno-González).

https://doi.org/10.1016/j.wroa.2026.100563
Received 19 January 2026; Received in revised form 26 May 2026; Accepted 28 May 2026
Available online 1 June 2026

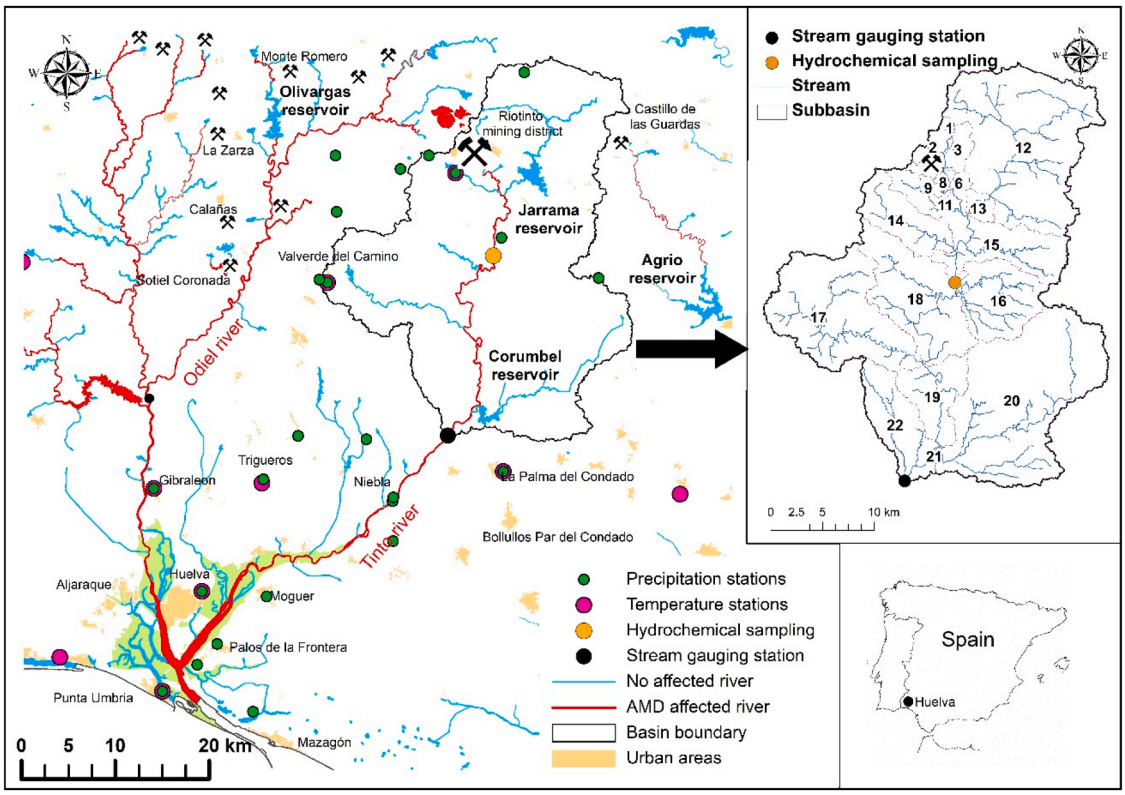

Fig. 1. Location map of the Tinto River and the Riotinto mining district, together with other mines in the area (AMD-affected watercourses are shown in red). The hydrochemical sampling point and the stream gauging station are indicated. Right: subbasins used in the hydrological model. Numbers shown in the upper-right panel correspond to subbasin identifiers (subbasins 4, 5, 7, and 10 are not shown because they are very small and spatially overlap with adjacent subbasins).

the neighboring Odiel River basin (e.g., Sánchez-España et al., 2005) and the shared estuary of both rivers (Cánovas et al., 2020; Sánchez-Moyano et al., 2025).

The Riotinto mine closed in 2000 due to an international decline in copper prices, which also affected many other mines in the IPB (Olías et al., 2024). Following the recovery of copper prices in international markets, the mine was reopened in 2015 with a commitment to eliminate acidic water discharges from wastes generated by historical mining activities. However, large areas covered by legacy mining wastes were excluded from the current exploitation project and therefore from the planned remediation measures.

The temporal evolution of dissolved concentrations in the Tinto River is complex and controlled by multiple interacting factors (Olías et al., 2020). These include climatic variability (seasonal to interannual changes in precipitation and temperature), the inputs from different AMD sources: open pits, underground workings, waste dumps and tailings (Cánovas et al., 2014), fine pyrite particles dispersed along the river bed and river bank (Gallego and Fernández-Caliani, 2023), the wash out of evaporite salts accumulated during dry periods (Cánovas et al., 2010), dilution by clean-water reservoir releases, and remediation actions implemented in the mining area. In Mediterranean climates, these dynamics are particularly abrupt due to strong variability in rainfall intensity (frequently >50 mm/day) and the rapid changes in river discharge and dissolved element concentrations that follow precipitation events (Galván et al., 2013). Beyond natural climatic variability, ongoing climate change in Mediterranean regions is expected to intensify summer droughts and increase the frequency of short, high-intensity rainfall events, potentially modifying contaminant storage and release dynamics in AMD-affected catchments.

Relationships between dissolved element concentrations and streamflow (C–Q) in river systems have been widely used to investigate the geochemical and hydrological processes controlling solute mobilization (e.g., Godsey et al., 2009; Hoagland et al., 2020; Jennings et al., 2025), to estimate pollutant loads (e.g., Galván et al., 2016), to assess the effectiveness of restoration measures (e.g., Newman et al., 2025), and to infer solute sources and groundwater transit times (Ibarra et al., 2016; Ameli et al., 2017).

In AMD-impacted catchments, most previous studies have either focused on short hydrochemical time series (such ass pH, electrical conductivity, and dissolved sulfate, metal and metalloid concentrations) or applied hydrological models without explicitly linking simulated discharge to long-term water-quality evolution. Consequently, the relative contributions of flow variability, climate-driven drying, and internal geochemical adjustment remain poorly constrained. Here, we apply the Soil and Water Assessment Tool (SWAT) model, a physically based, semi-distributed hydrological model, to reconstruct continuous daily discharge for the Tinto River and combine these simulations with a multi-year dataset of dissolved metal concentrations and concentration–discharge (C–Q) relationships. This integrated approach allows us to evaluate temporal shifts in river hydrochemistry under contrasting hydrological conditions. In this context, the main objective of this study is to assess the effect of the reopening of the Riotinto mine in 2015 on dissolved element concentrations in the Tinto River, based on the temporal evolution of hydrochemical data and the analysis of C–Q relationships.

2. Materials and methods

2.1. Study zone

The Tinto River is 101 km long and has a basin area of 1646 km^2. In the upper part of the basin the relief is formed by hills, with a maximum altitude of 680 m. In the lower part the terrain is smooth with altitudes lower than 50 m. The average river course slope is 0.4% and the average

altitude of the basin 159 m. The climate is Mediterranean, with mild and humid winters and warm, very dry summers. Mean annual temperature is close to 17 °C, with typical summer maxima of approximately 35 °C and occasional extremes approaching 40 °C in inland areas, and winter minima commonly around 0–1 °C in upland sectors (milder along the coast). Annual rainfall ranges from approximately 500 mm in the coastal area to approximately 800 mm in the headwaters. Rainfall is highly irregular both seasonally and interannually, with prolonged summer dry periods (often near-zero monthly rainfall) alternating with wetter autumn–winter conditions, when most of the annual precipitation is concentrated. This climatic regime promotes the seasonal accumulation of evaporitic salts during dry periods and their rapid leaching during the first rewetting events. A large part of the Tinto River basin runs through low-permeability rocks of the IPB, made up of three main geological units: 1) A thick sequence of slates and quartzites from the Upper Devonian, 2) The volcano-sedimentary complex, formed by an alternation of sediments and rocks from submarine volcanic eruptions of the Upper Devonian-Lower Carboniferous age, which store the large sulfide deposits that have been intensively exploited and, 3) The Culm group, made up of a turbidite sequence of slates and conglomerates from the Carboniferous (Olías et al., 2020).

In the Tinto basin there are two important reservoirs with good quality water, the Corumbel reservoir in the middle part with a capacity of 19 hm^3 and the Jarrama reservoir in the headwaters area, with a capacity of 48 hm^3 (Fig. 1).

2.2. Hydrochemical data

The water-quality sampling point is located in the upper reach of the Tinto River, 13 km downstream from the main mining area (Fig. 1). This station corresponds to the official water-quality monitoring network operated by the Andalusian Regional Water Authority (Junta de Andalucía) and is designed to receive the integrated hydrochemical signal from the Riotinto mining district. As such, it is representative of the cumulative acid mine drainage inputs affecting the upper segment of the river. Hydrochemical data were obtained from the Andalusian Regional Water Authority, which provides publicly accessible records (Junta de Andalucía, 2021). The dataset spans from May 2008 to December 2021 and includes a total of 90 samples. Sampling was conducted at approximately quarterly frequency throughout the study period, ensuring coverage of both dry and wet hydrological conditions. A data gap occurred between December 2015 and September 2016 due to the absence of measurements. From 2016 onwards, Cd, Ni, and Pb were monitored monthly, while the remaining parameters continued to be sampled quarterly.

Samples were filtered through 0.45-μm Millipore Teflon filters and subsequently acidified with suprapure HNO_3 Merk to pH < 1 and stored in the dark at 4 °C until analysis. Samples were analyzed by Inductively Coupled Plasma-Atomic Emission Spectroscopy (ICP-AES) for major elements, and by Inductively Coupled Plasma-Mass Spectroscopy (ICP-MS) for trace elements. The determination of sulfate was carried out using the internal method TM-M-010, which is based on the UNE-EN ISO 10,304–1 standard and employs ion chromatography. Detection limits were 1 mg/L for sulfate, Mg, Cu, Fe, Mn, and Zn and Fe and 3 μg/L for As, Cd, Cr, Ni and Pb. The precision and accuracy of the chemical analyses carried out within the Andalusian surface water monitoring network are ensured through laboratory accreditation in accordance with ISO/IEC 17,025 and the use of validated analytical methods with established measurement uncertainty estimation, being below 10% in all cases.

2.3. Hydrological modelling

Due to the lack of discharge data, the methodology employed in this study is based on hydrological modelling of the Tinto River basin to generate a continuous discharge dataset. This simulated discharge was integrated with hydrochemical data to explore the relationships between river flow and pollutant concentrations.

The hydrological simulations were conducted using the Soil and Water Assessment Tool (SWAT; Neitsch et al., 2005). SWAT is a physically based, semi-distributed hydrological model, which operates within the ArcGIS environment through an interface. The model calculates the daily water balance depending on the soil type, slope, land use, and weather data (temperature and precipitation). Potential evapotranspiration was estimated using the Penman–Monteith method. SWAT was selected because it provides continuous daily discharge at ungauged sites, allows explicit representation of topography/land cover/soil interactions, and has been successfully applied in AMD-affected basins (Galván et al., 2016).

The Digital Elevation Model (DEM), with a spatial resolution of 5×5 m, was used to delineate the watershed and drainage network. SWAT discretizes the basin into subbasins and Hydrologic Response Units (HRUs), unique combinations of land use, soil type, and slope, to simulate surface and subsurface processes. Input datasets included:

1. Daily weather data, including precipitation and maximum and minimum temperatures, were collected from 28 rain gauges and 13 temperature stations. The time series underwent a quality control process: anomalous values were corrected, and missing data were filled using linear regression based on nearby stations to ensure a consistent and complete dataset. SWAT uses elevations bands to calculate orographic precipitation. The daily precipitation in elevation bands is estimated by adding a constant amount to the recorded precipitation in the rain gauge, which depends on the increase in precipitation with altitude and the difference between the mean elevation of each band and the elevation of the recording gauge. This does not reflect rainfall in the subbasin because the increase in precipitation with altitude actually it is not constant, but depends on the amount of rainfall. Since SWAT does not accurately represent the spatial variability of precipitation associated with orographic effects (Galván et al., 2014), daily precipitation values were adjusted using an elevation-based correction factor. This factor accounts for the altitude difference between each rain gauge and the center of the corresponding elevation band (Galván et al., 2014).
2. The soils of the area were characterized by field samplings and laboratory analysis. Soil depth, percentage of clays, silts, sands and rock fragments, organic content, saturated hydraulic conductivity and bulk density were determined. Available water capacity (AWC) values were estimated based on soil texture and organic matter content using the formula developed by Saxton et al. (1986). Soil properties were derived from the regional soil survey of the province of Huelva developed by the University of Huelva (Domingo-Santos and Corral-Pazos-de-Provens, 2025), which includes 368 soil profile observations and additional field observations distributed throughout the province.
3. The land-use map was obtained from the Andalusian Environmental Agency based on official regional land classification data.

Model calibration and validation were performed using daily discharge data from a stream gauging station located at the middle part of the Tinto River (Fig. 1), covering the period from 2013 to 2021. Model performance was assessed through both visual inspection of simulated versus observed hydrographs and the computation of the following metrics: Pearson's correlation coefficient (r), the Nash–Sutcliffe efficiency coefficient (NSE; Nash and Sutcliffe, 1970), root mean square error (RMSE; Hogue et al., 2006), and runoff volume deviation (DV; Boyle et al., 2000).

2.4. Statistical treatment and concentration–discharge relationships

Statistical analyses were performed in R. The Shapiro–Wilk test (Shapiro and Wilk, 1965; R core team, 2024) was applied to evaluate the

normality of the discharge and hydrochemical variables (Table SM3). As most variables departed from a normal distribution, nonparametric tests were used to assess whether median values differed before and after the restarting of mining activity (2008–2014 and 2015–2021): the Wilcoxon rank-sum test (also known as the Mann–Whitney U test; Wilcoxon, 1945) and the Kruskal–Wallis test (Kruskal and Wallis, 1952). For both tests, the null hypothesis (H_0) was that median values did not differ between both periods, whereas the alternative hypothesis (H_1) was that they did.

The relationships between stream discharge and dissolved element concentrations were analyzed using the power-law equation $C = a \cdot Q^b$, where $C$is the dissolved concentration, $Q$is stream discharge, and $a$and $b$are empirical constants. This formulation is mathematically equivalent to a linear regression in log–log space, obtained by regressing $\log_{10}$ (C) against $\log_{10}$ (Q), with the slope corresponding to parameter b. Regressions were performed using SWAT-simulated discharge at the sampling point and observed dissolved concentrations. Only statistically significant relationships ($p < 0.05$) were considered. Following Godsey et al. (2009) and Jennings et al. (2025), C–Q relationships were classified as follows: (1) near-zero slopes ($-0.2 \leq b \leq 0.2$), indicating chemostatic behavior; (2) positive slopes ($b > 0.2$), indicating flushing or mobilization processes, with increasing concentrations as discharge rises; and (3) negative slopes ($b < -0.2$), indicating dilution, with decreasing concentrations as discharge increases.

3. Results and discussion

3.1. Hydrological modelling

From the DEM the basin was established until the stream gauging station (Fig. 1), with a surface of 808 km^2. Outlet points, defining the boundaries of each subbasin, were established at the sampling point, as well as at the confluences of the main tributaries. As a result, a total of 22 subbasins were delineated (Fig. 1).

The main land cover types in the watershed are scrublands (49% of the surface), range grasses (19%) and Eucalyptus forests (7%), reflecting a predominance of natural and semi-natural vegetation. A total of 18 soil types were identified within the watershed; their main physical and hydrological characteristics are summarized in Table SM1. Soils exhibit moderate clay content (11–31%), relatively high sand content (28–79%), and variable levels of rock fragments (4–60%). Most soils are shallow and poorly developed, with depths generally below 130 cm. According to the USDA Soil Taxonomy, Inceptisols are predominant, being the majority included within hydrologic group C. AWC values range from 10% to 42% by volume and saturated hydraulic conductivity from 0.29 to over 12 mm/day.

After integrating land use, soil type, and slope data into the model, the watershed was further subdivided into 1039 Hydrologic Response Units (HRUs). In SWAT, water balance processes are simulated at the HRU level, including surface runoff, infiltration, evapotranspiration, lateral flow, and percolation through the soil profile. Water percolating below the soil profile recharges a conceptual shallow aquifer storage, which contributes to streamflow as baseflow when the required storage conditions are met. A deep aquifer is also represented in the model, but recharge to this compartment is treated as a loss from the simulated catchment and does not directly contribute to streamflow. Thus, subsurface processes in SWAT are represented through conceptual storage reservoirs and transfer parameters rather than by prescribing a fixed physical aquifer depth.

Model calibration was conducted using discharge records from the stream gauging station (Fig. 1) for the period 2013–2019, while 2020–2021 was reserved for validation. Calibration was performed manually through a trial-and-error procedure, starting from the default SWAT parameterization. To reduce equifinality, only a limited set of hydrologically sensitive parameters was adjusted, while the remaining parameters were kept at their default values. The calibration focused on parameters controlling surface runoff generation, soil water balance, groundwater storage, and baseflow contribution to streamflow.

Table 1
Monthly and daily statistical indices for calibration and validation model of Tinto River (r: correlation coefficient; NSE: Nash–Sutcliffe's efficiency; RMS: root mean square error; and DV: runoff volume deviation).

	Calibration (oct 2013 - sept 2019)		Validation (oct 2019 - sept 2021)	
	Daily	Monthly	Daily	Monthly
r	0.82	0.98	0.91	0.96
NSE	0.66	0.95	0.83	0.88
RMS	4.71	0.89	1.61	0.48
DV	1.02	1.02	1.10	1.10

The adjusted parameters included the baseflow recession constant (ALPHA_BF), groundwater "revap" coefficient (GW_REVAP), initial water content in the shallow aquifer (SHALLST), threshold water depth in the shallow aquifer required for baseflow to occur (GWQMN), threshold water depth for "revap" to occur (REVAPMN), groundwater delay time (GW_DELAY), fraction of percolation to the deep aquifer (RCHRG_DP), SCS Curve Number (CN2), soil evaporation compensation factor (ESCO), and soil available water capacity (SOL_AWC). These parameters were modified using different calibration strategies depending on their role in the model structure. Some parameters were adjusted as additive or relative changes from their initial SWAT values, whereas others were modified as absolute values. Consequently, for parameters with spatially variable initial values, the same calibration strategy may lead to different final values among soil types, land uses, HRUs, or subbasins. The calibration strategy, default values, and final calibrated values are summarized in Tables SM5 and SM6.

Beyond the equifinality associated with model parameterization (already mitigated by restricting the set of adjusted parameters, as described above), a second source of equifinality stems from the fact that calibration in the present study relied on a single discharge gauging station located at the basin outlet (Fig. 1). While performance metrics such as NSE and RMSE indicate a good fit at this point, they do not constrain the internal hydrological behavior of the model across the catchment. With more than ten calibrated parameters per subbasin and a single calibration target, multiple parameter combinations can reproduce the observed discharge at the gauged location while differing substantially in how runoff, baseflow and groundwater recharge are partitioned upstream. This is illustrated by the fact that some parameters were assigned spatially uniform values across all HRUs (e.g., ALPHA_BF = 1, ESCO = 0.05), whereas baseflow generation and groundwater dynamics are known to vary considerably within watersheds (Eckhardt, 2005; Stewart et al., 2007; Cartwright, 2022; Zhong et al., 2022). Spatially uniform values therefore reflect calibration constraints rather than physical realism, and the simulated internal water balance should be interpreted accordingly.

To strengthen the constraint of distributed hydrological models in AMD-impacted basins such as the Tinto, future applications of this approach would benefit from collecting discrete discharge measurements at additional locations within the catchment, even sparse in time. These measures would substantially reduce parameter equifinality, and would benefit from adopting formal uncertainty quantification frameworks capable of explicitly characterizing the range of parameter sets compatible with the available observations. These considerations are particularly relevant for ungauged or sparsely gauged mining catchments, where the modeled discharge underpins downstream applications such as the C–Q analyses presented here.

Model performance was assessed through visual comparison of observed and simulated hydrographs together with statistical indicators, including the correlation coefficient (r), Nash–Sutcliffe efficiency (NSE), root mean square error (RMSE), and runoff volume deviation (DV). The monthly NSE reached 0.95 during the calibration period (Fig. SM1), which is classified as "very good" according to Moriasi et al. (2007)

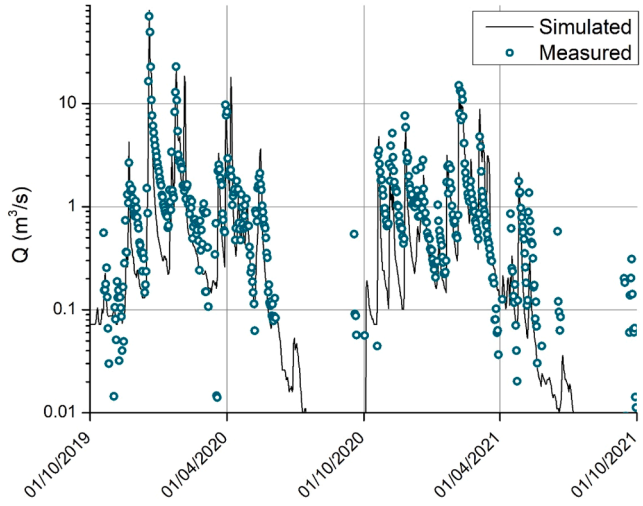

Fig. 2. Daily observed and simulated flows during the validation period. The calibration period is shown in Fig. SM1.

(Table 1). During validation, a good agreement between simulated and measured discharge was also observed (Fig. 2), with a monthly NSE value of 0.88, also within the "very good" category. Although the overall daily RMSE (4.11 m^3/s) is relatively high compared with the mean discharge (3.23 m^3/s), this metric is strongly influenced by a limited number of high-flow events. When considering discharge values below 5 m^3/s (approximately 94% of observations), RMSE decreases to 0.80 m^3/s, and for low flows ($Q < 1$ m^3/s), RMSE further decreases to 0.55 m^3/s. These discharge ranges correspond to most hydrochemical sampling conditions. Therefore, model performance is substantially stronger within the flow domain most relevant to the C–Q analysis.

Mean discharge for the period with hydrochemical data (2008–2021) was 3.23 m^3/s, with a maximum daily data of 186 m^3/s and minimum values close to zero during summers. Discharge shows sharp fluctuations as a result of precipitation events, indicating a low natural regulation capacity of the basin (Fig. 2). Given the strong calibration and validation performance, the simulated discharge series was considered reliable and subsequently used to compute the concentration–discharge (C–Q) relationships.

3.2. Hydrochemical characterization

The pH at the monitoring point remained very constant across the data set (range 2.1–3.0), with a median value of 2.5 (Tables 2 and SM7), due to strong buffering by Fe hydrolysis (Nordstrom et al., 2015). In contrast, electrical conductivity (EC) and dissolved element concentrations varied widely, with median values of 4.6 mS/cm for EC, 3.45 g/L for sulfate, 834 mg/L for Fe, 59 mg/L for Zn, 1.2 mg/L for As, among others (Table 2). The concentrations recorded in this study were higher than those reported in previous works (Cánovas et al., 2007; Olías et al., 2020). This was attributed to the position of the sampling point, where dilution from clean-water tributaries unaffected by AMD was limited.

No abrupt change was observed in the temporal evolution of dissolved concentrations following the reopening of the Riotinto mine in 2015 (Fig. 3 and Fig. SM2). However, the time series shows marked seasonal variability, which may affect the interpretation of long-term linear trends when the complete dataset is considered as a whole. To reduce this effect, temporal trends were evaluated separately for two subsets representing comparable hydrological conditions: (i) July–August samples, representative of low-flow summer conditions, and (ii) samples with discharge > 0.8 m^3/s, representative of high-flow conditions (Fig. 3). Under this approach, pH and most dissolved constituents, including sulfate, Cu, Mg, Mn, Zn, Cr and Ni, show stable to slightly decreasing trends through time. Fe shows a slight increasing trend, whereas As exhibits a more variable temporal behavior and Pb remains comparatively stable. Most dissolved elements generally behave conservatively, and their concentrations are mainly controlled by dilution due to inputs of waters not affected by AMD (Cánovas et al., 2007). By contrast, Fe, As and Pb exhibit a more complex hydrogeochemical behavior because they are influenced not only by dilution, but also by precipitation and coprecipitation processes (Acero et al., 2006; Nordstrom et al., 2015).

When comparing discharge and dissolved element concentrations before and after the restart of mining in 2015 (Table 2), the median values of EC, Fe, and Cd remained similar, whereas concentrations of the remaining elements in 2015–2021 were slightly lower than those recorded in 2008–2014. As dissolved concentrations do not follow a normal (Gaussian) distribution (Table SM3), the nonparametric

Table 2
Statistics of discharge and hydrochemical data obtained for the whole period (2008–2021) and dividing the data into two periods: from 2008 to 2014 and from 2015 to 2021. SD: Standard Deviation.

2008–21	Q m^3/s	pH	EC mS/cm	SO_4 mg/L	Cu mg/L	Fe mg/L	Mg mg/L	Mn mg/L	Zn mg/L	As µg/L	Cd µg/L	Cr µg/L	Ni µg/L	Pb µg/L
Data no.	90	49	50	50	45	46	65	46	49	47	86	45	87	87
Mean	1.26	2.5	5.0	4491	68	975	251	31	80	2226	315	58	389	232
Median	0.14	2.5	4.6	3457	57	834	189	26	59	1201	224	48	301	107
Min.	2E-04	2.1	1.2	148	7	21	13	2	6	113	5	13	10	4
Max.	27.0	3.0	9.9	15,673	176	2282	765	96	309	17,129	1196	163	1480	1641
SD	4.07	0.2	2.1	3628	43	598	179	22	60	3207	262	39	287	331
2008–14														
Data no.	23	22	23	23	18	19	23	19	20	20	19	17	20	20
Mean	2.36	2.6	5.1	5110	78	988	292	33	88	1940	340	68	518	216
Median	0.46	2.6	4.6	3876	77	839	232	27	69	1389	227	54	399	131
Min.	0.003	2.2	1.2	487	7	21	39	2	6	113	33	14	32	15
Max.	27.0	3.0	9.1	12,704	176	2200	765	71	186	7155	900	163	1480	685
SD	5.75	0.2	2.3	3247	48	654	212	24	59	1738	253	45	386	199
2015–21														
Data no.	67	27	27	27	27	27	42	27	29	27	67	28	67	67
Mean	0.88	2.5	5.0	3965	62	965	228	30	75	2437	308	52	350	236
Median	0.09	2.4	4.6	2490	53	830	189	26	59	956	220	45	275	107
Min.	2E-04	2.1	2.2	148	18	215	13	8	18	124	5	13	10	4
Max.	25.6	2.9	9.9	15,673	165	2282	721	96	309	17,129	1196	162	1048	1641
SD	3.29	0.2	2.0	3906	39	568	157	22	61	3984	265	34	240	362
Ratio 2015–21 respect to 2008–14														
Mean	0.38	1.0	1.0	0.8	0.8	1.0	0.8	0.9	0.8	1.3	0.9	0.8	0.7	1.1
Median	0.20	0.9	1.0	0.6	0.7	1.0	0.8	0.9	0.8	0.7	1.0	0.8	0.7	0.8

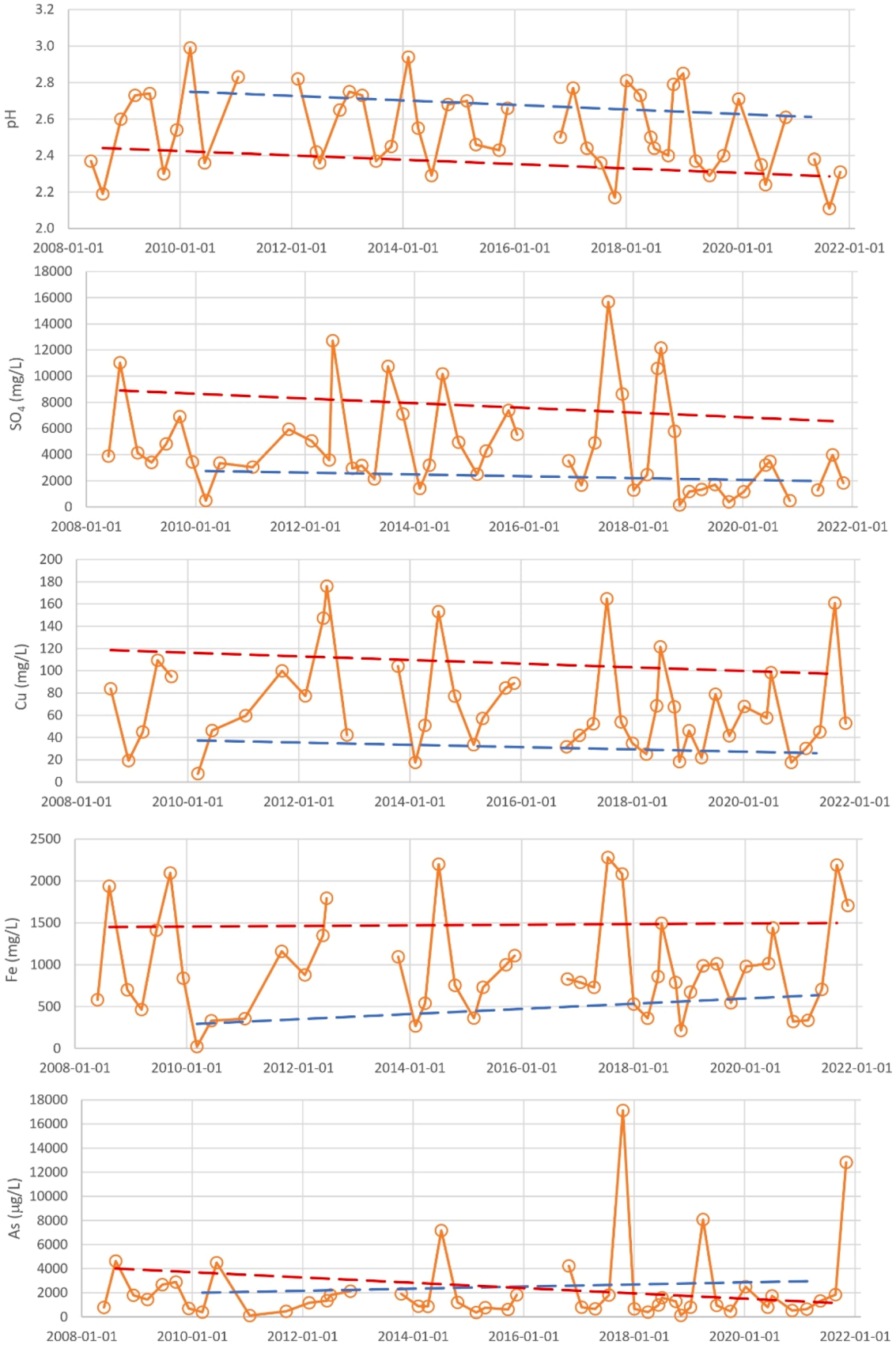

Fig. 3. Temporal evolution of selected hydrochemical variables at the monitoring site (see Fig. 1 for location). Orange lines and symbols show the measured values through time, whereas dashed lines represent linear trend fits for summer conditions (July–August, red) and high-flow conditions ($Q > 0.8$ m^3/s, blue).

Table 3
p values, R^2 and slope (b) for obtained CQ regressions (non-significant values at $p < 0.05$ are shown in bold).

	2008/14			2015/21		
	p value	R^2	b	p value	R^2	b
SO_4	<0005	0,63	−0,22	**0.075**	-	-
Cu	<0005	0,66	−0,24	<0005	0,61	−0,20
Fe	<0005	0,53	−0,32	<0005	0,29	−0,15
Mg	<0005	0,60	−0,26	<0005	0,56	−0,25
Mn	<0005	0,67	−0,32	<0005	0,64	−0,25
Zn	<0005	0,61	−0,28	<0005	0,43	−0,24
As	<0.05	0,13	−0,16	**0.84**	-	-
Cd	<0005	0,39	−0,22	<0005	0,36	−0,24
Cr	<0.005	0,69	−0,23	<0005	0,55	−0,18
Ni	<0005	0,45	−0,28	<0005	0,52	−0,23
Pb	<0.05	0,24	0,17	<0005	0,10	0,32

Wilcoxon and Kruskal–Wallis tests (see Section 2.4) were applied to assess whether these differences were statistically significant. For all variables, p-values exceeded 0.05 (Table SM4), and the null hypothesis of equal medians between periods could not be rejected. This indicates that, despite the apparently lower concentrations in 2015–2021, the differences between periods are not statistically resolved given the sample size and the high temporal variability of the dataset.

However, it should be noted that the 2008–14 period was much wetter than the 2015–21 period, such that the median river discharge was five times lower in the latter period (ratio 0.20 in Table 2). Differences in precipitation can influence the contributions of surface and underground AMD generation sources in the mining area. However, in Mediterranean climates, there are two very contrasting seasons: winter with lower temperatures and high rainfall rates, and summer with high temperatures and a lack of rainfall. Although the pollutant load increases during the rainy season, the concentrations decrease due to runoff generated in areas unaffected by mining. Conversely, in summer we have the highest concentrations because less dilution runoff freshwaters along with a higher rate sulfide weathering exist (e.g. Olías et al., 2006; Manning et al., 2024). This leads to intense precipitation of efflorescent salts, which temporarily store sulfates and metals, but are subsequently washed away during the first significant rainfall event of autumn. Despite the high dissolved concentrations, pollutant loads during the dry season are the lowest of the year, because streamflow is minimal. A similar pattern is observed when comparing dry and wet years, dissolved concentrations increase whereas transported loads decrease, while the opposite occurs during wet years.

3.3. Concentration–discharge relationships

Acid mine drainage sources in mining areas commonly exhibit chemostatic or flushing behavior for elements such as Zn, SO_4, and Fe, indicating that concentrations remain relatively invariant across several orders of magnitude of discharge variation (Newman et al., 2025). In contrast, stream waters often display dilution patterns, with negative slopes for most constituents due to mixing with less concentrated runoff water (Langmuir, 1997). Nevertheless, AMD-impacted streams may occasionally show flushing behavior associated with the mobilization of evaporitic salts precipitated during dry periods (Olías et al., 2006; Newman et al., 2025).

Almost all regressions between flow and dissolved concentrations found were statistically significant at a confidence level of $p < 0.005$ (Table 3). The only non-significant regressions were sulfate ($p = 0.07$) and arsenic ($p = 0.84$) for the 2015/21 period. For most elements, regressions showed a clear dilution pattern with slopes (b parameter) lower than −0.2. Arsenic, Cr, Fe and Pb present a chemostatic pattern ($-0.2<b<0.2$) in some period. The only element that exhibits flushing behavior is Pb during the period 2015–2021, with a slope value of +0.32 (Table 3, Fig. 4). This contrasting trend for Pb reflects its complex hydrochemical behavior. In addition to coprecipitation with Fe minerals, dissolved Pb concentrations are controlled by the solubility of anglesite and other Pb-bearing sulfates, leading to higher Pb concentrations when sulfate levels decrease (Cánovas et al., 2007).

In summary, two groups of elements could be distinguished. First, those that exhibit conservative behavior in the acidic water of the Tinto River (sulfates, copper, magnesium, manganese, zinc, cadmium, and nickel). The CQ relationships of these compounds show a dilution pattern, indicating that their concentration is controlled by inputs from the mining area together with dilution from runoff from areas unaffected by mining. Their temporal evolution shows a downward trend due to the decrease in mining inputs since 2015. The second group consists of Fe, As and Pb, which, in addition to the processes mentioned above, are subject to precipitation/coprecipitation processes and exhibit more complex hydrogeochemical behavior. These elements do not exhibit a decreasing trend in concentration over time and the CQ relationships generally exhibit a chemostatic behavior with $b < 0.2$ (for Pb in the period 2015/2021 it is even increasing) and/or lower R^2 values.

On the other hand, based on the daily flow data obtained by SWAT and the regressions shown in Fig. 4, the pollutant load of the different elements with statistically significant values was calculated. A significant reduction in the pollutant load was observed. For example, for copper, the median value for the period 2008–2014 was 980 kg/day, and for the period 2015–2021, it was 595 kg/day. This decrease could be due to reduced rainfall. Nevertheless, it is verified that, for the same flow rate, the dissolved concentrations for the period 2015/21 are lower than those of 2008/14. For example, for a flow rate of 1 m^3/s, the regression equations obtained concentrations of 42 mg/L, 174 µg/L, and 35 µg/L for Cu, Cd, and Cr in the period 2008/14, while the values for the period 2015/21 are 33 mg/L, 117 µg/L, and 28 µg/L, respectively. The only elements that do not follow this trend are Pb and Fe for flow rates greater than approximately 0.1 m^3/s, due to their complex hydrogeochemical behavior as commented above (for As, the regression for the period 2015–21 was not statistically significant).

The identification of well-documented case studies explicitly evaluating the effects of mine reopening on river water quality remains limited in literature. Research on acid mine drainage (AMD) has predominantly focused on legacy or abandoned mining sites characterized by chronic contamination, as well as on processes associated with mine closure, flooding of underground workings. For instance, Herbst et al. (2018) evaluated the long-term effects of acid mine drainage (AMD) on streams of California (USA), reporting a slow recovery, depending on factors such as the magnitude and duration of contamination, hydrological conditions, natural attenuation capacity, and the implementation of remediation measures (e.g., source control, active or passive treatment systems). In contrast, the impact of reactivation of previously closed mines on the quality of already mining affected watercourses have been scarcely documented and is more commonly addressed within environmental impact assessments, regulatory submissions, consultancy reports, and other forms of grey literature. Therefore, given the scarcity of peer-reviewed studies on the impact of mine reopening on river water quality, this study provides novel insights into the hydrogeochemical response of AMD-affected systems to restarted mining activity. By quantitatively comparing pre- and post-reopening conditions, it helps fill a critical knowledge gap in the literature. The results have important implications for environmental risk assessment and mine management in regions considering reactivation of legacy sites.

In addition to natural seasonal and interannual variability, ongoing climate change is expected to intensify the hydrochemical contrasts between dry and wet periods in AMD-affected systems such as the Tinto River. In Mediterranean regions, projections point to longer and more intense summer droughts together with an increasing frequency of short, high-intensity rainfall events. These shifts are likely to enhance the seasonal accumulation of evaporitic salts during prolonged dry periods and to promote more abrupt first-flush contaminant pulses during rewetting events. As a result, climate-driven changes in hydrological

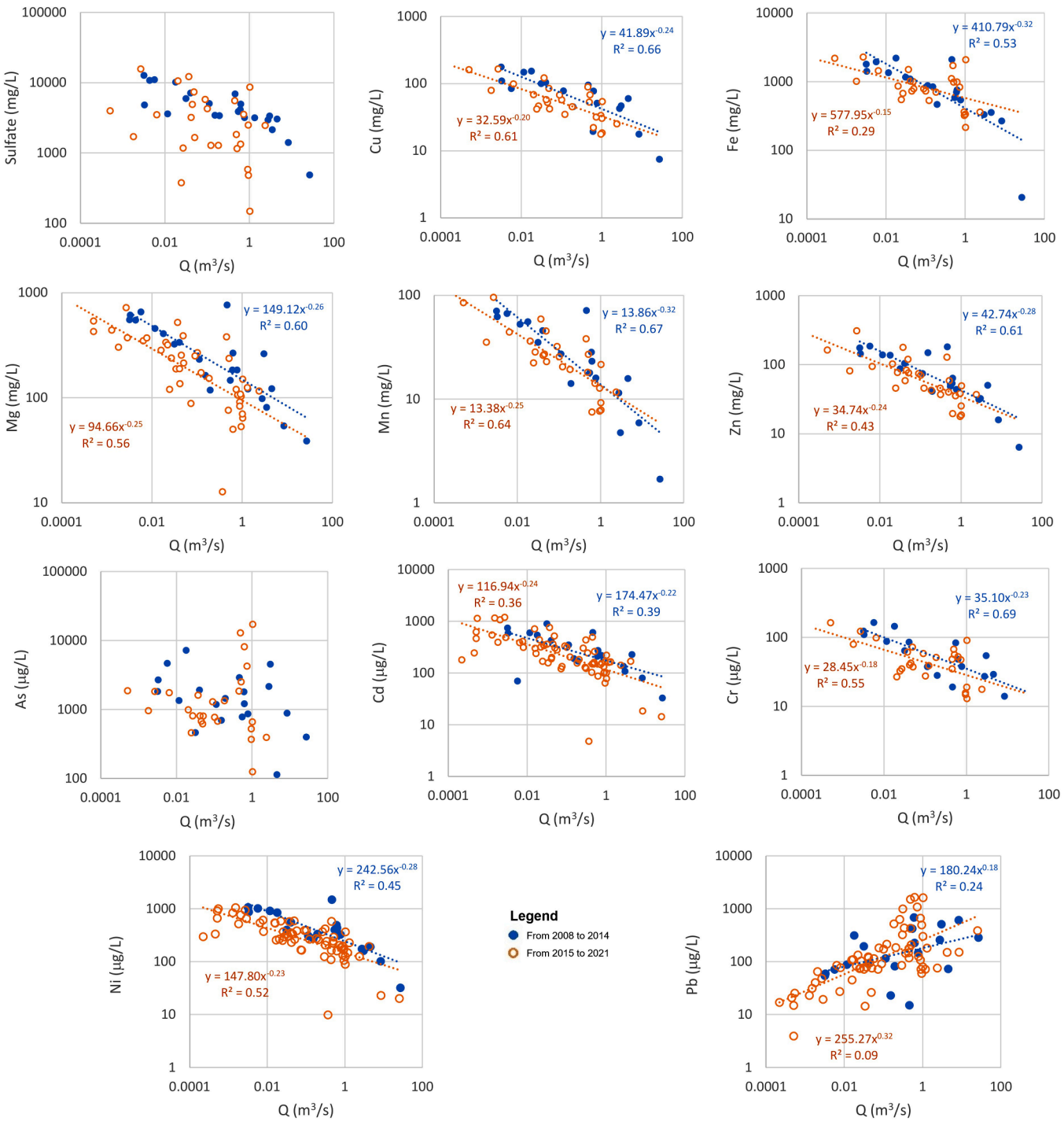

Fig. 4. Concentration–discharge (CQ) relationships. Blue circles represent 2008–2014 and orange circles represent 2015–2021. Regression lines for sulfate and As in 2015–2021 are omitted because they are not significant ($p > 0.05$).

regimes may mask or amplify the effects of remediation measures, complicating the interpretation of long-term hydrochemical trends and concentration–discharge relationships.

4. Conclusions

The SWAT-based hydrological modeling provided a good agreement with observed discharge data in the Tinto River, accurately capturing the sharp fluctuations driven by rainfall due to the basin's low natural regulation capacity. The post-2015 period, following the resumption of mining activity, was notably drier, with discharge values about five times lower than in 2008–2014.

Despite these drier conditions, dissolved element concentrations did not increase, indicating an overall improvement in water quality after the mine reopening. Most elements exhibited slight downward trends, whereas Fe and As showed moderate increases and Pb remained stable. These differences reflect the strong influence of precipitation and coprecipitation processes on Fe, As, and Pb, which govern their more complex hydrochemical behavior.

Although nonparametric tests did not detect statistically significant differences in median concentrations between both periods, the absence of a concentration increase under markedly drier conditions in

2015–2021 is consistent with reduced pollutant inputs from the mining area. Concentration–discharge (CQ) relationships displayed a dominant dilution pattern, with concentrations decreasing as discharge increased.

Overall, the recommissioning of the Riotinto mine and the partial remediation of historical acid drainage sources have led to measurable water-quality improvements, even under less favorable (drier) hydrological conditions. These findings highlight the importance of integrating hydrological variability into the assessment of restoration effectiveness. Furthermore, the potential influence of ongoing climate change must be explicitly considered, as it can either mask or amplify anthropogenic remediation efforts and thus affect the long-term sustainability of AMD-impacted systems.

The concentration–discharge (CQ) analysis highlights how mine reopening altered the river's geochemical dynamics. Changes in CQ behavior for metals and sulfate reveal shifts in solute sources and flow-dependent mobilization that simple load calculations alone cannot capture. By distinguishing hydrogeochemically controlled (Fe, As and Pb) versus conservative solutes (sulfate, Cu, Mg, Mn, Zn, etc.), CQ analysis provides a more nuanced understanding of watershed response to human-driven actions.

Data availability

Hydrochemical data are available from the Andalusian Regional Water Authority. The SWAT model input files, calibrated parameters, and model output data supporting this study are publicly available in HydroShare: Moreno Gonzalez, R. (2026). ArcSWAT Proyect Tinto Basin, HydroShare, http://www.hydroshare.org/resource/b72952fc07564c02b426e8a6e16182fa.

CRediT authorship contribution statement

Raúl Moreno-González: Writing – original draft, Visualization, Validation, Methodology, Investigation, Formal analysis, Data curation, Conceptualization. **Manuel Olías:** Writing – review & editing, Supervision, Methodology, Funding acquisition, Conceptualization. **Carlos R. Cánovas:** Writing – review & editing, Supervision, Resources, Investigation, Funding acquisition. **Laura Galván:** Writing – review & editing, Methodology. **Rubén Fernández de Villarán:** Writing – review & editing, Data curation.

Declaration of competing interest

The authors declare that they have no known competing financial interests or personal relationships that could have appeared to influence the work reported in this paper.

Acknowledgments

This research was supported by the Spanish Ministry of Science and Innovation through grant FJC2021-047600-I, funded by the Spanish State Research Agency (AEI) and the European Union–NextGenerationEU. Additional support was provided by grant DGP_POST_2024_00813, funded by the Junta de Andalucía/CUII and the European Social Fund Plus (ESF+), and by the Programa de Fomento de la Actividad Investigadora of the University of Cádiz. This work was also funded by the European Union through the project Critical Ecosystems in Mining Sites – CEMIS. WP1 Sensor networker – 1A1 Water Resources and Climate Change (Ref. LIFEWATCH-2019-04-AMA-01), and by the RECUP-DAS project, co-funded by the European Union through the European Regional Development Fund (ERDF) under the Andalucía FEDER Programme 2021–2027. Open access publication was supported by the Plan Propio–UCA 2025–2027 of the University of Cádiz. We are grateful to two anonymous reviewers for their valuable suggestions, which significantly improved the original manuscript.

Supplementary materials

Supplementary material associated with this article can be found, in the online version, at doi:10.1016/j.wroa.2026.100563.

References

Acero, P., Ayora, C., Torrento, C., Nieto, J.M., 2006. The behavior of trace elements during schwertmanite precipitation and subsequent transformation into goethite and jarosite. Geochim. Cosmochim. Acta 70, 4130–4139. https://doi.org/10.1016/j.gca.2006.06.1367.

Ameli, A.A., Beven, K., Erlandsson, M., Creed, I.F., McDonnell, J.J., Bishop, K., 2017. Primary weathering rates, water transit times, and concentration-discharge relations: a theoretical analysis for the critical zone. Water. Resour. Res. 53, 942–960. https://doi.org/10.1002/2016WR019448.

Boyle, D.P., Gupta, H.V., Sorooshian, S., 2000. Towards improved calibration of hydrological models: combining the strengths of manual and automatic methods. Water. Resour. Res. 36, 3663–3674. https://doi.org/10.1029/2000WR900207.

Cánovas, C.R., Olías, M., Nieto, J.M., Sarmiento, A.M., Cerón, J.C., 2007. Hydrogeochemical characteristics of the Odiel and Tinto rivers. Factors controlling metal contents. Sci. Total Environ. 373, 363–382. https://doi.org/10.1016/j.scitotenv.2006.11.022.

Cánovas, C.R., Olías, M., Nieto, J.M., Galván, L., 2010. Wash out processes of evaporitic sulfate salts in the Tinto River: hydogeochemical and environmental impact. Appl. Geochem. 25, 288–301. https://doi.org/10.1016/j.apgeochem.2009.11.014.

Cánovas, C.R., Olias, M., Nieto, J.M., 2014. Metal(loid) attenuation processes in an extremely acidic river: the Rio Tinto (SW Spain). Water, Air, Soil Pollut. 225, 1795. https://doi.org/10.1007/s11270-013-1795-7.

Cánovas, C.R., Basallote, M.D., Borrego, P., Millán-Becerro, R., Pérez-López, R., 2020. Metal partitioning and speciation in a mining-impacted estuary by traditional and passive sampling methods. Sci. Total. Environ. 722, 137905. https://doi.org/10.1016/j.scitotenv.2020.137905.

Cartwright, I., 2022. Implications of variations in stream specific conductivity for estimating baseflow using chemical mass balance and calibrated hydrograph techniques. Hydrol. Earth. Syst. Sci. 26 (1), 183–195. https://doi.org/10.5194/hess-26-183-2022.

Domingo-Santos, J.M., Corral-Pazos-de-Provens, E., 2025. Suelos forestales de la provincia de Huelva: propiedades, evolución y distribución territorial. Ed. Universidad de Huelva Col. Alonso Barba 23. https://hdl.handle.net/10272/25208.

Eckhardt, K., 2005. How to construct recursive digital filters for baseflow separation. Hydrol. Process. 19 (2), 507–515. https://doi.org/10.1002/hyp.5675.

Gallego, L., Fernández-Caliani, J.C., 2023. Pyrite ore cargo spills as a source of soil pollution and ecological risk along the abandoned railway corridors of the Tharsis and Rio Tinto mines (Spain). Environ. Monit. Assess. 195, 97. https://doi.org/10.1007/s10661-022-10715-3.

Galván, L., Olías, M., Cerón, J.C., Cánovas, C.R., Pérez- López, R., Nieto, J.M., 2013. Assessment of the dissolved pollutant flux of the Odiel River (SW Spain) during a wet period. Sci. Total Environ. 463-464, 572–580. https://doi.org/10.1016/j.scitotenv.2013.06.067.

Galván, L., Olías, M., Izquierdo, T., Cerón, J.C., Fernández de Villarán, R., 2014. Rainfall estimation in SWAT: an alternative method to simulate orographic precipitation. J. Hydrol. 509, 257–265. https://doi.org/10.1016/j.jhydrol.2013.11.044.

Galván, L., Olías, M., Cánovas, C.R., Sarmiento, A.M., Nieto, J.M., 2016. Hydrological modeling of a watershed affected by acid mine drainage (Odiel River, SW Spain). Assessment of the pollutant contributing areas. J. Hydrol. 540, 196–206. https://doi.org/10.1016/j.jhydrol.2016.06.005.

Grande, J.A., Valente, T., de la Torre, M.L., Santisteban, M., Cerón, J.C., Pérez-Ostalé, E., 2014. Characterization of acid mine drainage sources in the iberian pyrite belt: base methodology for quantifying affected areas and for environmental management. Environ. Earth. Sci. 71, 2729–2738. https://doi.org/10.1007/s12665-013-2652-0.

Godsey, S.E., Kirchner, J.W., Clow, D.W., 2009. Concentration-discharge relationships reflect chemostatic characteristics of US catchments. Hydrol. Process. 23, 1844–1864. https://doi.org/10.1002/hyp.7315.

Herbst, D.B., Medhurst, R.B., Black, N.J.P., 2018. Long-term effects and recovery of streams from acid mine drainage and evaluation of toxic metal threshold ranges for macroinvertebrate community reassembly. Environ. Toxicol. Chem. 37, 2575–2592. https://doi.org/10.1002/etc.4217.

Hoagland, B., Navarre-Sitchler, A., Cowie, R., Singha, K., 2020. Groundwater-stream connectivity mediates metal(oid) geochemistry in the hyporheic zone of streams impacted by historic mining and acid rock drainage. Front. Water. 2, 600409. https://doi.org/10.3389/frwa.2020.600409.

Hogue, T.S., Gupta, H.V., Sorooshian, S., 2006. A "user-friendly" approach to parameter estimation in hydrologic models. J. Hydrol. 320, 202–217. https://doi.org/10.1016/j.jhydrol.2005.07.009.

Ibarra, D.E., Caves, J.K., Moon, S., Thomas, D.L., Hartmann, J., Chamberlain, C.P., Maher, K., 2016. Differential weathering of basaltic and granitic catchments from concentration–discharge relationships. Geochim. Cosmochim. Acta 190, 265–293. https://doi.org/10.1016/j.gca.2016.07.006.

Jennings, E., Onnis, P., Crane, R., Comber, S.D.W., Byrne, P., Riley, A.L., Mayes, W.M., Jarvis, A.P., Hudson-Edwards, K.A., 2025. Spatial and temporal (annual and decadal) trends of metal(loid) concentrations and loads in an acid mine drainage-affected river. Sci. Total Environ. 964, 178496. https://doi.org/10.1016/j.scitotenv.2025.178496.

Junta de Andalucía, 2021. Datos de calidad de las aguas. Consejería de Sostenibilidad y Medio Ambiente. https://www.juntadeandalucia.es/medioambiente/portal/areas-tematicas/agua/calidad-aguas-y-control-de-vertidos/datos-de-calidad-de-las-agua.

Kruskal, W.H., Wallis, W.A., 1952. Use of ranks in one-criterion variance analysis. J. Am. Stat. Assoc. 47 (260), 583–621. https://doi.org/10.1080/01621459.1952.10483441.

Langmuir, D., 1997. Aqueous Environmental Geochemistry. Prentice Hall, Upper Saddle River.

Manning, A.H., Petach, T.N., Runkel, R.L., McKnight, D.M., 2024. Climate-driven increases in stream metal concentrations in mineralized watersheds throughout the colorado rocky mountains, USA. Water. Resour. Res. 60, e2023WR036062. https://doi.org/10.1029/2023WR036062.

Moriasi, D.N., Arnold, J.G., van Liew, M.W., Bingner, R.L., Harmel, R.D., Veith, T.L., 2007. Model evaluation guideleines for systematic quantification of accuracy in watershed simulations. Trans. ASABE 50 (3), 885–900. https://doi.org/10.13031/2013.23153.

y Nash, J.E., Sutcliffe, J.V., 1970. River flow forecasting through conceptual models 1. A discussion of principles. J. Hydrol. 10, 282–290. https://doi.org/10.1016/0022-1694(70)90255-6.

Neitsch, S.L., Arnold, J.G., Kiniry, J.R., Williams, J.R., 2005. Soil and water assessment tool. Theoretical documentation. Version 2005. Texas Water Resources Institute Report TR-191, p. 494.

Newman, C.P., Navarre-Sitchler, A., Runkel, R.L., Cowie, R., 2025. Concentration-discharge relations and transient metal loads reveal spatiotemporal variability in solute-generation mechanisms in a mine-affected watershed. J. Contam. Hydrol. 269, 104513. https://doi.org/10.1016/j.jconhyd.2025.104513.

Nordstrom, D.K., Blowes, D.W., Ptacek, C.J., 2015. Hydrogeochemistry and microbiology of mine drainage: an update. Appl. Geochem. 57, 3–16. https://doi.org/10.1016/j.apgeochem.2015.02.008.

Olías, M., Cánovas, C.R., Nieto, J.M., Sarmiento, A.M., 2006. Evaluation of the dissolved contaminant load transported by the Tinto and Odiel rivers (South West Spain). Appl. Geochem. 21, 1733–1749. https://doi.org/10.1016/j.apgeochem.2006.05.009.

Olías, M., Cánovas, C.R., Macías, F., Basallote, M.D., Nieto, J.M., 2020. The evolution of pollutant concentrations in a river severely affected by acid mine drainage: río Tinto (SW Spain). Minerals 10, 598. https://www.mdpi.com/2075-163X/10/7/598#.

Olías, M., Cánovas, C.R., Basallote, M.D., Macías, F., Nieto, J.M., Pérez-López, R., Sarmiento, A.M., 2024. The problem of acid mine drainage in the iberian pyrite belt (IPB). diagnosis and treatment measures. ed. publication service of the university of huelva. https://www.uhu.es/publicaciones/?q=libros&code=1347.

R Core Team, 2024. R: A language and Environment For Statistical Computing. R Foundation for Statistical Computing, Vienna, Austria. https://www.R-project.org/.

Sánchez España, J., López Pamo, E., Santofimia, E., Aduvire, O., Reyes, J., Barettino, D., 2005. Acid mine drainage in the iberian pyrite belt (odiel river watershed, huelva, sw spain). geochemistry, mineralogy and environmental implications. Appl. Geochem. 20, 1320–1356. https://doi.org/10.1016/j.apgeochem.2005.01.011.

Sánchez-Moyano, E., Rodríguez-Muñoz, D., García-Asensio, I., 2025. Evaluating environmental programs: long-term monitoring of crustacean assemblages in a polluted estuary. Estuaries Coasts 48, 1. https://doi.org/10.1007/s12237-024-01449-1.

Saxton, K.E., Rawls, W.J., Romberger, J.S., Papendich, R.I., 1986. Estimating generalizad soil-water characteristics from texture. Soil Sci. Soc. Am. J. 50, 1031–1036. https://doi.org/10.2136/sssaj1986.03615995005000040039x.

Shapiro, S.S., Wilk, M.B., 1965. An analysis of variance test for normality (complete samples). Biometrika 52 (3–4), 591–611. https://doi.org/10.1093/biomet/52.3-4.591.

Stewart, M., Cimino, J., Ross, M., 2007. Calibration of base flow separation methods with streamflow conductivity. Ground. Water. 45 (1), 17–27. https://doi.org/10.1111/j.1745-6584.2006.00263.x.

Wilcoxon, F., 1945. Individual comparisons by ranking methods. Biom. Bull. 1 (6), 80. https://doi.org/10.2307/3001968.

Zhong, Y., Hu, J., Zhang, J., Mo, Q., 2022. Optimal baseflow separation scheme considering both high precision and low cost — take major watersheds in the United States as an example. J. Hydrol. 612, 128133. https://doi.org/10.1016/j.jhydrol.2022.128133.